Volume 5 | Number 12 | 21 June 2018

ORGANIC CHEMISTRY

FRONTIERS

Chinese Chemical Society

rsc.li/frontiers-organic

ORGANIC CHEMISTRY
FRONTIERS

RESEARCH ARTICLE

View Article Online
View Journal | View Issue

Cite this: *Org. Chem. Front.*, 2018, **5**, 1877

The design of rigid cyclic tripyrrins: the importance of intermolecular interactions on aggregation and luminescence†

Jun-Fei Wang,‡[a] Yuhang Yao,‡[b] Yingying Ning,[b] Yin-Shan Meng,[b] Chun-Liang Hou,[a] Jing Zhang *[a] and Jun-Long Zhang *[b]

Received 27th March 2018,
Accepted 10th April 2018

DOI: 10.1039/c8qo00313k

rsc.li/frontiers-organic

We designed a cyclic tripyrrin "locked" by a bridging benzene-1,4-diol-moiety which is perpendicular to the tripyrrin plane. The cyclic structures promote the scaffold rigidity and enhance the fluorescence. While the halogen-substitution of the bridging moiety was found to slightly affect the fluorescence of **1–3** in solution, such substitution significantly affects the aggregation behaviour and solid emission. **1** and **2** exhibit typical *J*-aggregate emission but **3** does not. The analysis of crystal packing combined with the reduced density gradient (RDG) analysis suggests that the bridging moieties of **1–3** play an important role in inducing the different crystal packing by tuning intermolecular interactions in the solid state. The energy decomposition analysis using symmetry adapted perturbation theory (SAPT) revealed that such weak intermolecular interactions mainly consist of halogen bonds and π–π interactions.

Introduction

Tripyrrin and their derivatives are important core components of naturally occurring linear oligopyrroles such as biopyrrins and biotripyrrins *a* and *b*, which are regarded as the biodegradation products of hemin and chlorophylls.[1] The unique T-shaped tripyrrin structures attracted increasing attention in coordination chemistry as non-innocent ligands,[1d,2] in medicinal chemistry as biological ion acceptors or transporters,[3] and in synthetic chemistry as building blocks for expanded porphyrins.[4] Despite tremendous progress made in recent years, the photophysical properties of tripyrrins have been much less studied, probably due to the conformational flexibility. It is evident that chelating Zn^{2+} ions to α-tripyrrinone significantly enhances the fluorescence, which is assumed to increase the structural rigidity, as reported by Xie and co-workers.[5] Thus, with the target to construct the rigid tripyrrins, we believe that using the covalent bond to "lock" pyrrolic terminals is an effective approach. It is envisaged that the use of the bridging moiety would enhance the rigidity, while fine-tuning of the substitution of the bridging moiety can impart steric congestion and thus the alignment of intermolecular interactions.

The alignment of organic molecules through intermolecular interactions has pivotal effects on their macroscopic properties.[6] Commonly, organic fluorophores are highly emissive in dilute solutions, but become weakly luminescent or even non-emissive in the aggregate state due to the aggregation-caused quenching (ACQ) effect, which has limited the practical application of organic fluorophores.[7] Introducing sterically hindered groups vertical to chromophores can achieve *J*-aggregation for some classic dye molecules such as cyanine, squaraines, and perylene bisimide derivatives.[8] *J*-Aggregation leads to the couplings of transition dipoles and facilitates the delocalization of the excited state over multiple chromophores and thus bathochromically shifts the absorption/emission spectra, which have attracted much attention for fundamental studies and potential applications.[8b,9] However, designing molecular structures to form slipped stacks is not enough, fine-tuning of weak intermolecular interactions such as hydrogen bonds, halogen bonds and π–π stacking is also significant in designing and even controlling molecular aggregation.[8b,10]

Herein, we report the synthesis of fluorescent cyclic tripyrrins bridged by benzene-1,4-diol, which is perpendicular to the tripyrrin plane. Notably, with the enhanced rigidity offered by annulation, this work represents the first report of enhancing luminescence without metal chelation in tripyrrin and its derivatives.[5a,11] Other than the emission in solution, the substitution of the bridging benzyl moiety plays a critical role in tuning the aggregation and emission in the solid state,[12]

[a]*College of Materials Science and Optoelectronics Technology, University of Chinese Academy of Sciences, Beijing 100049, P. R. China. E-mail: zhangj271@ucas.ac.cn*
[b]*Beijing National Laboratory for Molecular Sciences, State Key Laboratory of Rare Earth Materials Chemistry and Applications, College of Chemistry and Molecular Engineering, Peking University, Beijing 100871, P.R. China. E-mail: zhangjunlong@pku.edu.cn*

† Electronic supplementary information (ESI) available. CCDC 1581723–1581725. For ESI and crystallographic data in CIF or other electronic format see DOI: 10.1039/c8qo00313k

‡ These authors contributed equally to this work.

which is highly related to intermolecular π–π stacking and halogen bond interactions. This work opens a new access to design functional cyclic oligopyrroles by incorporating a perpendicular bridging moiety, which shows the prospective to modulate functions in the solid state by tuning weak intermolecular interactions.

Results and discussion

Synthesis and characterization

Starting from pentafluorophenyltripyrrane, **1–3** were obtained in the overall yields of *ca.* 40% *via* a two-step process. Firstly, tripyrrane was treated with 2 equiv. of *N*-bromosuccinimide (NBS) in THF at −78 °C for 1 h. After the treatment of $Na_2S_2O_3$ solution, the brominated intermediates were obtained. Further oxidation together with cross-link coupling was achieved by the treatment of different quinones in CH_3CN at r.t. or 80 °C, as shown in Scheme 1. The crude products were subjected to silica gel column chromatographic purification, which afforded the desired products **1–3** as orange solids. **1–3** were characterized using HR ESI-MS, ^{1}H, ^{13}C and ^{19}F NMR, FT-IR spectrometry and spectroscopy (Fig. S1–S12†). The steric configurations were further confirmed by single crystal X-ray diffraction. The ^{1}H-NMR spectra of **1–3** exhibiting β-proton signals appear as three peaks in the range of 5.8–6.8 ppm (Fig. S1–S3†). **1** and **2** only downfield shifted the β-protons about 0.05 ppm compared with **3**, indicating the slight effect of electron-withdrawing cyano-substitution of the bridged moiety. The ^{13}C- and ^{19}F-NMR spectra showed the similar signal patterns of **1** and **2**, but slightly different from those of **3** (Fig. S4–S9†).

X-ray crystallography

Single crystals of **1** (CCDC 1581723†) and **2** (CCDC 1581724†) were obtained by slow diffusion of hexane into a tetrahydrofuran solution, and the crystal of **3** (CCDC 1581725†) was obtained by the diffusion of methanol into a chloroform solution. Importantly, these crystal structures show a larger tilt of the benzene ring compared with the reported *p*-benziporphyrin (Fig. S13–S15 and Tables S1–S3†).[13] Taking **1** as an example, the tripyrrole part (N_3-plane) is "locked" to be a flat plane. As shown in Fig. 1a, the phenyl ring is almost perpendicular to the N_3-plane with a dihedral angle of 83°. **2** and **3** possess similar configurations with a dihedral angle of 86° and 85° between the bridged phenyl ring and the N_3-plane (Fig. 1b and c). Notably, the cavity of a macrocycle is considerably larger than *p*-benziporphyrin. The N1–N2, N2–N3 and N1–N3 distances are 3.012, 3.012 and 4.371 Å, respectively. These large cavities are disadvantageous for metal coordination. These results clearly suggest the rigidity and uniqueness of cyclic tripyrrins arising from benzene-1,4-diol covalently "locked" terminal pyrroles, different from the previously reported benziporphyrin analogues.

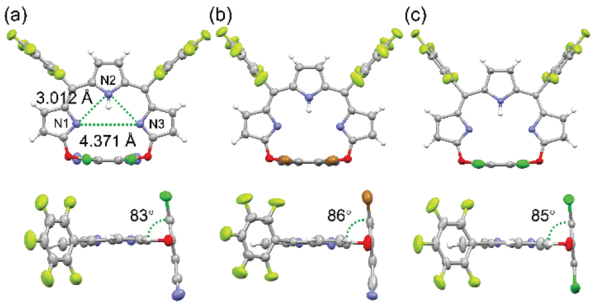

Fig. 1 X-ray crystal structures of **1–3** (a)–(c). Top view (top) and side view (bottom). The thermal ellipsoids are set to 50% probability.

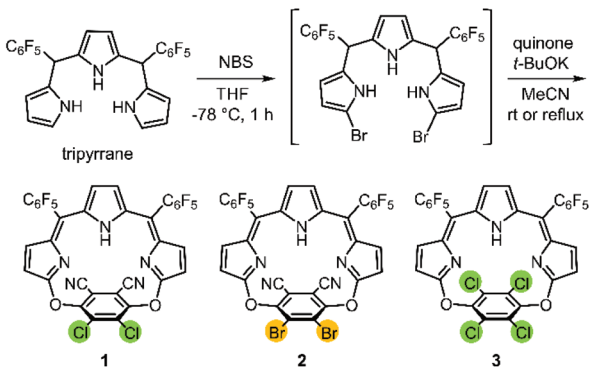

Scheme 1 Synthetic method of cyclic tripyrrins **1–3**.

Electrochemical properties

To investigate the electrochemical properties of **1–3**, we performed cyclic voltammograms in CH_2Cl_2 using 0.10 M *n*-Bu_4NPF_6 as the supporting electrolyte. As shown in Fig. S16–S18,† all three compounds have two distinct reversible reductions at *ca.* −1.24 and −1.53 V, and one reversible oxidation around *ca.* 1.05 V, referenced to the standard potential of Fc^+/Fc. This indicated that the bridging phenyl moiety, even with different electronic effects arising from the substitution, is irrelevant to the frontier molecular orbitals. To gain further insight into their electronic structures, density functional theory (DFT) calculations have been performed to optimize the structures of **1–3** and calculate the energy at the B3LYP[14] level with a 6-31G(d) basis set[15] using the Gaussian 09 package.[16] The HOMO and LUMO of **1–3** localize in the tripyrrin part. While the LUMO+1 of **3** still persists in the tripyrrin side, the orbitals of **1** and **2** shift to the benzene ring due to the electron-withdrawing nature of substituents (Fig. S19†). The energy difference between the HOMO and LUMO levels of **1** and **2** remains at 0.03 eV, and this value is elevated to 0.2 eV for **3** (Table S4†). These results clearly demonstrate that the bridging phenyl moiety only endows the structures of tripyrrin with more rigidity and slightly changes the energy levels or electronic structures.

Photophysical properties

As shown in Fig. 2a, the UV-vis spectra of **1–3** in CH_2Cl_2 exhibited three intense absorbances centered at *ca.* 319, 500 and

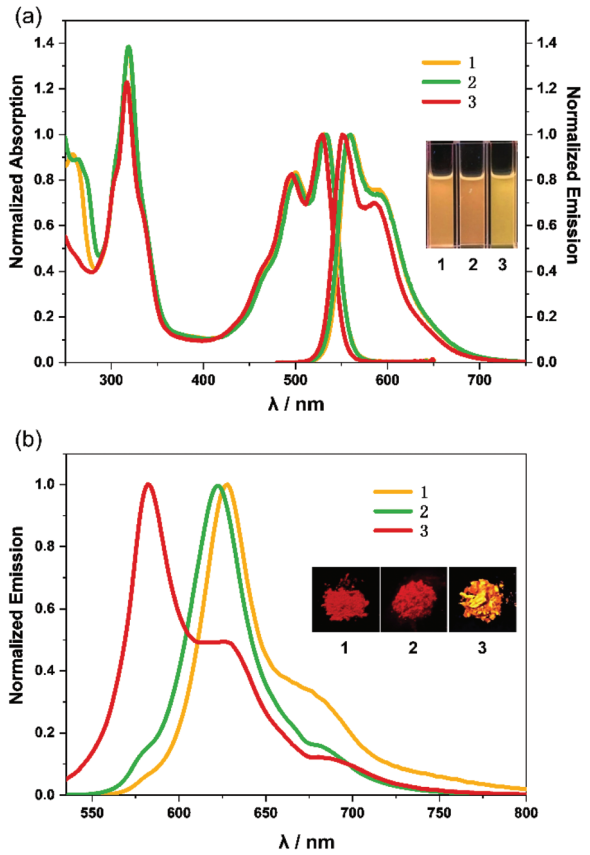

Fig. 2 (a) Absorption and emission spectra of **1–3** in CH_2Cl_2 solution; (b) emission spectra of **1–3** in the solid state. Insert: Photographs taken under the 365 nm UV lamp.

530 nm, which are slightly affected by the substitution of the bridging moiety. The absorption spectra of compounds **1–3** were also recorded in poly(methyl methacrylate) (PMMA) films, which are similar to those in dilute solution. As shown in Fig. S20,† **1–3** displayed two intense absorption bands centered 318 nm in the range of 300–400 nm and 530 nm with two shoulders at 466 and 500 nm in the range of 410–650 nm in PMMA films. TDDFT computational data indicate that the vertical excitation at 530 nm of **1–3** from the S_0 to S_1 state is a local excitation of π–π* (HOMO → LUMO, 100%), and the excitation of **1–3** at 319 nm has contributions from several other excitation configurations (Tables S5–S7†). For **1** and **2**, the excitation at 500 nm should be a charge transfer transition (HOMO → L+1, 99.8%) from the S_0 to S_2 state with essentially near zero oscillator strength. For **1** and **2**, the vertical transition involves mainly the HOMO to LUMO transition localized on the tripyrrin core, while the LUMO+1 involved in the S_0 to S_2 transition is localized in the phenyl which is perpendicular to the tripyrrin plane (Fig. S19†). However, for **3**, the excitation at 500 nm cannot be assigned according to TDDFT calculations.

Upon excitation in the dilute solution of CH_2Cl_2, **1–2** display strong emission with a maximum of 560 nm with a shoulder at *ca.* 590 nm, while **3** shows a slight blue-shift of 9 nm compared with **1** and **2**. No apparent difference was observed on their photoluminescence in solution, as shown in the inserted photographs of Fig. 2a. The quantum yields (QYs) of **1–3** are 8.2, 7.3 and 8.5%, respectively, referred to fluorescein, considerably higher than the previously reported tripyrrin ligands (non- fluorescence or weak fluorescence).[2c,11,17] The fluorescence lifetimes for **1–3** are about 0.7 ns (Fig. S21–S23 and Table S8†). A more prominent increase in fluorescence is attributed to the rigid structures of cyclic tripyrrins, comparable to the effect arising from chelating metal ions.[5a] It is worth noting that similar spectroscopic changes observed for **1–3** suggest that the electronic structures in both ground and excited states are much less dependent on the choice of the bridging moiety.

Significantly, unlike conventional organic fluorophores that are usually non-emissive in the solid state, **1** and **2** emit red fluorescence in the solid state with λ_{max} at 622 and 627 nm and a shoulder at *ca.* 680 nm (with QYs of 3.8 and 2.4% respectively, Fig. S24 and S25†). However, **3** shows orange emission centered at 582 nm and two shoulders at 629 and 682 nm with a QY of 3.1% (Fig. S26†), as shown in Table 1 and Fig. 2b. The λ_{max}s of solid-state emission are bathochromically shifted by 68 nm and 62 nm for **1** and **2**, while only 31 nm for **3** relatively to those of the dilute solution (Fig. 3a–c). Under the irradiation of a 365 nm UV lamp, **1** and **2** are red emission solids and **3** emits orange as shown in the inset photographs in Fig. 2. Other than solid states, **1–3** also show concentration-dependent emissions in CH_2Cl_2. As shown in Fig. 3d, e and f, **1–3** undergo bathochromic shifts along with the concentration increasing from 10^{-5} M to 10^{-3} M in CH_2Cl_2. These results clearly suggest that intermolecular interactions play an important role in influencing aggregation and photophysical properties through comparison of **1–3**.

J-Aggregation

To illustrate the intermolecular interactions in **1–3**, we analyzed the π-stacking and slip angles by comparing their crystal packing, as shown in Fig. 4 and S27–S29.† For **1**, the two head-to-tail stacked molecules are separated by 5.72 Å, while the interplanar distances between the tripyrrin units of two partially stacked neighbouring molecules are 3.19 and 2.53 Å, respectively. The slip angles of molecules **1** in the crystal lattice are about 21.0 and 12.3°, much less than 54.7°.[18] **2** has

Table 1 Fluorescent peak (FL/nm) and quantum yields (QY/%) of **1–3** in different states

	1	2	3
FL/nm and QY/% in CH_2Cl_2 solution[a]	560 (8.2%)	560 (7.3%)	551 (8.5%)
FL/nm and QY/% in crystals[b]	627 (3.8%)	622 (2.4%)	582 (3.1%)
FL/nm in amorphous form	586	613	604, 666
FL/nm and QY/% doped in PMMA films[b]	615 (1.6%)	615 (5.1%)	615 (5.0%)

[a] Fluorescein as a reference and excited at 470 nm. [b] Absolute quantum yields.

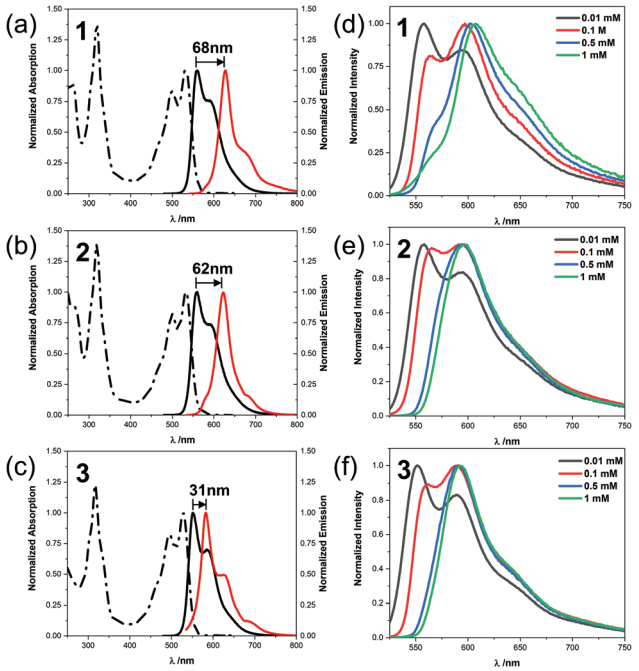

Fig. 3 Absorption (dot dashed line) and emission spectra (solid line) of **1–3** (a)–(c) in CH_2Cl_2 (blue) and as powder (red). Emission spectra of **1–3** (d)–(f) at concentrations of 10^{-5} M to 10^{-3} M in CH_2Cl_2.

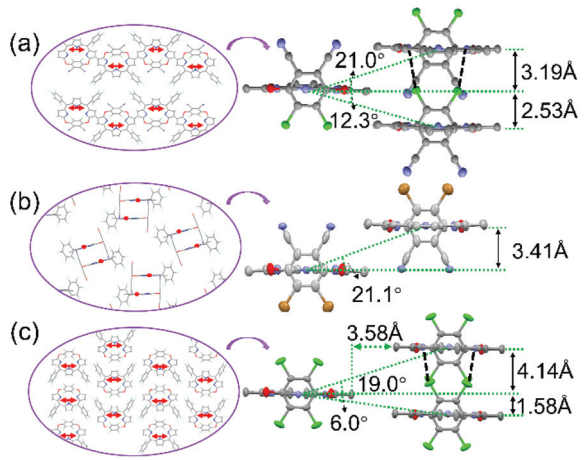

Fig. 4 Crystal packing and aggregation dimers in **1** (a), **2** (b) and **3** (c). The bidirectional red arrows and dots indicate the transition dipole moment in the left panel, and the black dash lines represent the N···Cl contact.

a tilted aggregation dimer as **1** with slip angles of 21.1° and interplanar distances of 3.41 Å. However, the packing between the dimers in the crystal of **2** is non-parallel, which is different from **1** and **3**. The slip angles in **3** are 19.0 and 6.0°, and the interplanar distances are 4.14 and 1.58 Å. But the intermolecular distance along the long axial direction (parallel to the N_3-plane) is 3.58 Å, which is significantly larger than that in **1** and **2** and indicates that the units of the pair in **3** are much separated. It is well-known that in order to form *J*-aggregates, the slip angle defined by the transition dipole and the stacking axis is required to be less than 54.7°. Thus, **1** and **2** likely show *J*-aggregation behavior as the slip angles are much less than 54.7°, while **3** may not show *J*-aggregation behavior due to the long intermolecular distance between dimers.

To test this hypothesis, we compared the fluorescence of the crystalline and amorphous states of **1–3**, which are important to investigate the effect of packing behavior on the photophysical properties of **1–3** (Table 1). As shown in Fig. S30 and S31,† the fluorescence of **1** and **2** was partially or completely quenched after grinding in a crucible, and then recovered after evaporating from CH_2Cl_2 solution. However, grinding in a crucible did not significantly change the fluorescence emission of **3**. The different fluorescence of **1** and **2** between crystalline and amorphous states further indicates the importance of aggregation (or *J*-aggregation) on their photophysical properties. **3** exhibited much smaller changes of fluorescence in the amorphous state likely due to the different packing pattern from that in **1**. In addition, we also measured the fluorescence of **1–3** doped with PMMA films (Fig. S32–S35†), which might reflect their photophysics by reducing intermolecular interactions in the solid matrix. As shown in Table 1 and Fig. S32,† the emission of **1–3** is *ca.* 615 nm and showed much less difference than those in crystalline states, but similar to those in solution.

To further confirm the formation of *J*-aggregation, we studied the effect of aggregation by varying the fraction of water (f_w, by volume) in DMSO–water mixed solvents. **1–3** have good solubility in common organic solvents including dimethyl sulfoxide (DMSO) but poor solubility in water. As shown in Fig. 5a, for **1**, at f_w of 0% to 30%, the absorption spectrum shows almost no change by keeping the concentration at *ca.* 50 μM. However, at f_w of 32%, the monomer absorption peaks at 498 and 533 nm of **1** decrease dramatically and a new broad absorption band at around 575 nm emerges. Similarly, the monomer emission peaks of **2** decrease and a new peak at 564 nm appears at f_w of 50% (Fig. 5b). The emission of **1** and **2** red-shifts from 570 to 600 nm with a shoulder at 625 and 570 to 590 nm with a shoulder at 630 nm, respectively (Fig. 5d and e), by increasing f_w from 0% to 100%. These spectral changes indicated the typical formation of *J*-aggregates due to the bathochromically shifted narrow absorption or emission. In contrast, varying the fraction of water did not change the shape of the absorption of **3**, and only quenches the emission intensity (Fig. 5c and f). These spectral changes in absorption and emission suggested that compound **3** does not form *J*-aggregates. The red-shifts in the emission band of **3** in the solid state may be simply due to reabsorption,[19] which is a common phenomenon in measuring fluorescence from molecular crystals, and the bathochromically shifted value of **3** is also much smaller than that of **1** and **2**.

Weak interaction analysis

To further gain insight into intermolecular interactions from the crystal packing of **1–3**, we took the reduced density gradi-

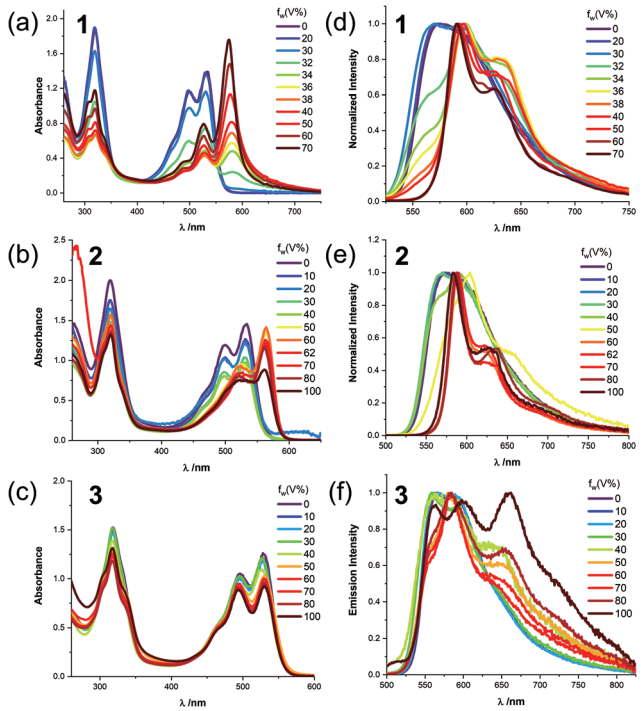

Fig. 5 (a)–(c) Absorption and (d)–(f) normalized emission spectra of **1–3** at a concentration of 50 μM in DMSO–water mixed solvents.

ent analysis (RDG)[20] at the level of B3LYP[14]/6-31G(d).[15] In the axial direction of crystals in **1** and **3**, a weak contact was observed between the N and Cl atoms of two stacked molecules of **1** and **3** with a distance of 3.20, 3.56 Å and 3.57, 3.64 Å, respectively (Fig. 6a and c), and similar interactions (3.57 Å) between two Cl atoms were also found in **3** (Fig. 6c). **1** and **2** show the formation of π–π interactions in the *J*-type aggregation dimers (Fig. 6a and b), and **1** also exhibits weak π–π interactions between pentafluorophenyl groups (Fig. 6a). The tilted stacking pattern of **1–3** results from the steric congestion of the perpendicular bridging moiety. However, the halogen bonds of N–Cl and Cl–Cl in **1** and **3** shorten the distance (5.72 Å) of head-to-tail stacked molecules from the perpendicular direction of the N_3-plane (Fig. 4a, c, 6a, c and S36†) and thus form the parallel packing pattern. The π–π interaction between the pentafluorophenyl groups of **1** shortens the intermolecular distance from the parallel direction of the N_3-plane (Fig. 6a and S36†), and forms *J*-aggregation in **1**. However, for **3**, the lack of π–π interactions between the pentafluorophenyl groups enlarges the intermolecular distance (3.58 Å) in the parallel direction (Fig. 6c and S36†). Thus the molecules **3** are too apart to form *J*-aggregation. In addition, the large distance (5.72 Å) between tripyrrin units from the perpendicular direction prevents the formation of *H*-aggregation (Fig. 4c and 6c). For **2**, bromine-substitution of the bridging moiety weaken the formation of the halogen bond, and the lack of the halogen bond in the perpendicular direction of the N_3-plane and π–π interactions in the parallel direction induce a loose and non-parallel crystal packing (Fig. 4b and 6b). But the π–π interaction between tripyrrin units drives the formation of *J*-aggregation in dimers (Fig. 6b). Thus, the detailed information by the RDG analysis suggests that the different weak interactions in **1–3** induced the different crystal packing and thus photophysical properties in the solid state.

Quantitative results were also obtained by energy decomposition analysis using symmetry adapted perturbation theory (SAPT)[21] on **1–3**. As shown in Fig. 7, the dispersion force (*ca.* −15 to −18 kcal mol^{-1}), which is often attributed to the π–π interaction, contributes most to the binding of **1** and **2**, and the electrostatic stabilization is about two-thirds of the former (*ca.* −9 to −12 kcal mol^{-1}). Induction, at −2 to −3 kcal mol^{-1}, provides the remaining stabilization. These results confirm the formation of *J*-aggregation in **1** and **2** again. In contrast, only dispersion has a little effect (−0.8 kcal mol^{-1}) on **3**, and the total binding can also be neglected compared with **1** and **2**, which further indicate the negligible intermolecular interaction in the crystal of **3**. Therefore, the quantitative analysis of SAPT further suggests that different weak interactions consist of halogen bonds and π–π interactions.

Experimental section

Solvents and reagents were used as received. UV/Vis spectra were recorded with an Agilent 8453 UV/Vis spectrometer equipped with an Agilent 89090 A thermostat (±0.1 °C) at 25 °C. ^{1}H, ^{19}F, ^{13}C NMR spectra and all the isomerization experiments were recorded on Bruker ARX 400 instrument at

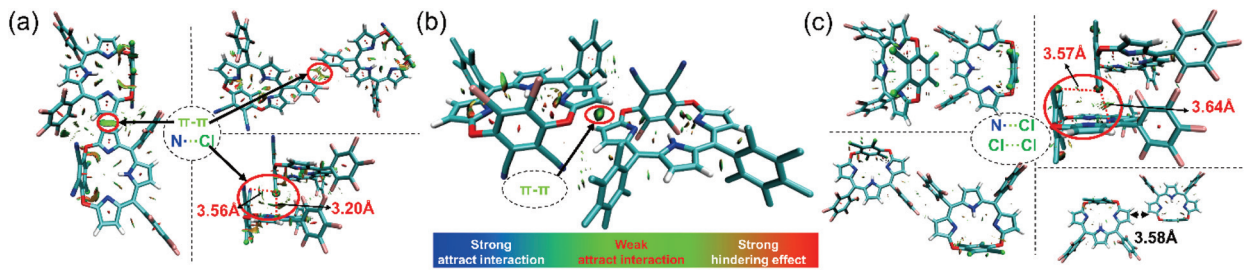

Fig. 6 Reduced density gradient (RDG) analysis with an isovalue of 0.50 in three axial directions for **1** (a), **2** (b) and **3** (c), which shows the weak attractive interactions (green blocks in red cycles) of π–π stacking and the corresponding N···Cl (3.20 and 3.56 Å) for **1**, and only N···Cl (3.57 and 3.64 Å) for **3**.

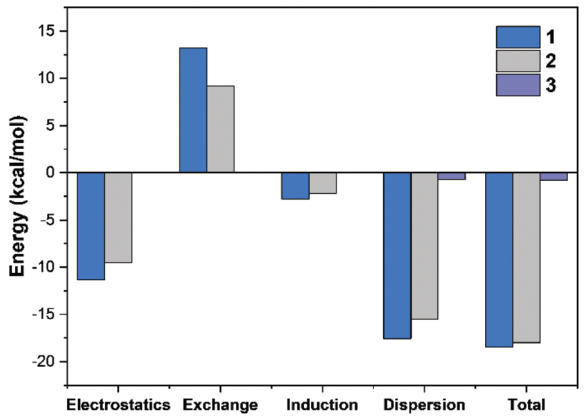

Fig. 7 Energy decomposition analysis to show the energy components of aggregation dimers of **1–3**.

298 K. High and low resolution mass spectra were provided by the Mass Spectrometry Facilities at the University of Connecticut and Peking University. IR spectra were acquired in KBr pellets using a Bruker VECTOR22 FT-IR spectrometer. Emission spectra and lifetime measurements were recorded on an Edinburgh Analytical Instruments FLS920 lifetime and a steady-state spectrometer (450 W Xe lamp/microsecond flash lamp, PMT R928 for the visible emission spectrum). Quantum yields in solution were determined using a comparative method and the equation: $\Phi_s/\Phi_r = (G_s/G_r) \times (\eta_s^2/\eta_r^2)$, where the subscripts r and s denote the reference and the sample, respectively, Φ is the quantum yield, G is the slope from the plot of integrated emission intensity *vs.* absorbance, and η is the refractive index of the solvent.[22] The reference was fluorescein 0.1 M NaOH solution ($\Phi_r = 0.925$, $\lambda_{ex} = 470$ nm).[22] The absolute quantum yields in the solid state and PMMA films were determined on an Edinburgh Analytical Instrument FLS-980 equipped with an integrating sphere. Intensity data of crystals were collected on a Bruker Smart ApexII CCD diffractometer with graphite-monochromated Mo Kα radiation (0.71073 Å) at 180 K or 277 K. The structures were solved by direct methods and refined with the full-matrix least-squares technique based on F^2 using the SHELXL program. All non-hydrogen atoms were refined anisotropically. Hydrogen atoms were placed at the calculation positions.

Synthesis of 1

N-Bromosuccinimide (128.5 mg, 0.72 mmol) was dissolved in dry THF (10 mL), and added dropwise to pentafluorophenyltripyrrane (200 mg, 0.36 mmol) in dry THF (10 mL) at −78 °C. The reaction was monitored by TLC and quenched with aqueous $Na_2S_2O_3$. The organic layer was extracted with DCM and dried over anhydrous Na_2SO_4. After evaporation under reduced pressure, the residue was dissolved in CH_3CN (10 mL) and DDQ (244.5 mg, 1.08 mmol) was added. The reaction was continued for 12 h, monitored by TLC. After evaporation under reduced pressure, the residue was subjected to a silica column directly and separated with an eluent of PE : DCM = 3 : 1. The desired product **1** was obtained as a red powder (90 mg, 32%). ^{1}H NMR (400 MHz, chloroform-d) δ 10.30 (s, 1H), 6.73 (d, J = 4.8 Hz, 2H), 6.64 (d, J = 4.8 Hz, 2H), 5.99 (d, J = 2.4 Hz, 2H); ^{19}F NMR (377 MHz, chloroform-d) δ −137.79 (ddd, J = 23.2, 8.7, 4.4 Hz), −138.70 (ddd, J = 23.4, 8.7, 4.4 Hz), −151.09 (t, J = 21.0 Hz), −159.99 (td, J = 22.2, 8.4 Hz), −160.39 (td, J = 22.2, 8.4 Hz); ^{13}C NMR (101 MHz, chloroform-d) δ 175.28, 151.64, 146.20, 138.70, 136.27, 136.13, 121.56, 119.41, 119.00, 111.36, 110.56. UV-vis (CH_2Cl_2): λ_{max} [nm] ($\varepsilon \times 10^{-4}$) = 319 (5.09), 498 (3.07) and 533 (3.64); HRMS (ESI) m/z found 777.98905, calcd 777.98899 for $C_{34}H_8Cl_2F_{10}N_5O_2$ ($[M + H]^+$).

Synthesis of 2

N-Bromosuccinimide (128.5 mg, 0.72 mmol) was dissolved in dry THF (10 mL), and added dropwise to pentafluorophenyltripyrrane (200 mg, 0.36 mmol) in dry THF (10 mL) at −78 °C. The reaction was monitored by TLC and quenched with aqueous $Na_2S_2O_3$. The organic layer was extracted with DCM and dried over anhydrous Na_2SO_4. After evaporation under reduced pressure, the residue was dissolved in CH_3CN (10 mL) and 2,3-dibromo-5,6-dicyano-1,4-benzoquinone (340 mg, 1.08 mmol) and *t*BuOK (80 mg, 0.72 mmol) was added. The reaction was continued for 2 h at 90 °C, and then chloranil (177 mg, 0.72 mmol) was added to oxidize the material and compound **2** appeared as an orange red point on the TLC plate. The reaction was continued for further 5 h, and then evaporated under reduced pressure. The residue was subjected to the silica column directly and separated with the eluent of PE : DCM = 5 : 1. The desired product **2** was obtained as a red powder (136 mg, 43.5%). ^{1}H NMR (400 MHz, chloroform-d) δ 10.29 (s, 1H), 6.73 (d, J = 4.8 Hz, 2H), 6.64 (d, J = 4.8 Hz, 2H), 6.00 (d, J = 2.4 Hz, 2H); ^{19}F NMR (377 MHz, chloroform-d) δ −137.75 (ddd, J = 23.5, 8.5, 4.5 Hz), −138.70 (ddd, J = 23.4, 8.8, 4.6 Hz), −151.17 (t, J = 20.8 Hz), −160.04 (td, J = 22.1, 8.5 Hz), −160.47 (td, J = 22.1, 8.5 Hz); ^{13}C NMR (101 MHz, chloroform-d) δ 175.35, 152.49, 146.29, 138.63, 136.28, 129.75, 121.50, 119.29, 119.15, 111.76, 110.79. UV-vis (CH_2Cl_2): λ_{max} [nm] ($\varepsilon \times 10^{-4}$) = 319 (4.90), 500 (2.88) and 533 (3.53); HRMS (ESI) m/z found 865.88818, calcd 865.88796 for $C_{34}H_8Br_2F_{10}N_5O_2$ ($[M + H]^+$).

Synthesis of 3

N-Bromosuccinimide (128.5 mg, 0.72 mmol) was dissolved in dry THF (10 mL), and added dropwise to pentafluorophenyltripyrrane (200 mg, 0.36 mmol) in dry THF (10 mL) at −78 °C. The reaction was monitored by TLC and quenched with aqueous $Na_2S_2O_3$. The organic layer was extracted with DCM and dried over anhydrous Na_2SO_4. After evaporation under reduced pressure, the residue was dissolved in CH_3CN (10 mL) and chloranil (265 mg, 1.08 mmol) was added. The reaction was continued for 12 h at 90 °C, monitored by TLC. After evaporation under reduced pressure, the residue was subjected to the silica column directly and separated with the eluent of PE : DCM = 8 : 1. The desired product **3** was obtained as an orange powder (65 mg, 23%). ^{1}H NMR (400 MHz, chloroform-

d) δ 10.42 (s, 1H), 6.67 (d, J = 4.8 Hz, 1H), 6.60 (d, J = 4.8 Hz, 1H), 5.93 (d, J = 2.4 Hz, 1H); ^{19}F NMR (377 MHz, chloroform-d) δ −138.30 to −138.51 (m), −151.78 (t, J = 20.8 Hz), −160.62 (td, J = 21.0, 6.3 Hz); ^{13}C NMR (101 MHz, chloroform-d) δ 174.79, 146.77, 146.31, 137.98, 136.11, 127.71, 120.68, 119.53, 117.82. UV-vis (CH_2Cl_2): λ_{max} [nm] ($\varepsilon \times 10^{-4}$) = 317 (4.18), 495 (2.82) and 528 (3.39); HRMS (ESI) m/z found 795.92330, calcd 795.92055 for $C_{32}H_8Cl_4F_{10}N_3O_2$ ($[M + H]^+$).

Electrochemistry measurement

The electrochemical experimental procedures were conducted with a standard three electrode configuration on a Shanghai Chenhua CHI660C electrochemical workstation at room temperature, 25 °C, under argon. Cyclic voltammetry experiments were recorded using glassy-carbon working electrode disks of 3 mm diameter (Cypress Systems EE040). The working electrode was treated between scans by means of a sequence of polishing with diamond paste (Buehler) of decreasing sizes (3 to 0.05 μm) interspersed by washings with purified H_2O. The auxiliary electrode was a platinum wire electrode and the Ag/AgCl electrode was the reference electrode. All glassware for electrochemical experiments was oven dried overnight and allowed to cool to room temperature before use.

Calculation details

The Gaussian 09 software package (version D.01)[16] was used for all the geometry optimization at the B3LYP[14]/6-31G(d)[15] level, and the TDDFT calculations were performed for the optimized structures of the ground state at the same level. The reduced density gradient (RDG) analysis[20] was performed for selected dimers using Multiwfn 3.4.1[23] and plotted using VMD 1.9.3,[24] and the selected dimers were pre-calculated at the level of B3LYP[14]/6-31G(d)[15] in Gaussian 09[16] to obtain electron density. The energy decomposition analysis was carried out using symmetry adapted perturbation theory (SAPT)[21] in the open-source *ab initio* Electronic Structure Package PSI 4.0.0-beta5 driver (SAPT0, paired with the jun-cc-pVDZ basis set).[25]

Conclusions

In summary, we reported the design and synthesis of cyclic tripyrrins with benzene-1,4-diol as a bridging moiety. Single crystal structures showed the bridging benzyl moiety perpendicular to the tripyrrin plane, endowing the whole molecular structures with rigidity. As expected, the fluorescence of tripyrrins is significantly enhanced, however, it is irrelevant to the substitution of the bridging benzyl moiety. Interestingly, the halogen-substitution of the bridging moiety significantly affects the solid emission, which is related to the halogen bonds and π–π interactions. Both **1** and **2** exhibit typical *J*-aggregate emission, while **3** emits fluorescence only due to the different crystal packing in the solid state. Thus, RDG analysis suggests that the bridging moieties of **1–3** are important to induce the different crystal packing and thus photophysical properties in the solid state. SAPT analysis suggests that there are halogen bonds and π–π interactions involved in the crystalline states. Therefore, this work enriches the repertoire of oligopyrrole and opens access to design functional oligopyrroles by tuning weak intermolecular interactions by the perpendicular bridging moiety.

Conflicts of interest

There are no conflicts to declare.

Acknowledgements

We thank the National Key Basic Research Support Foundation of China (NKBRSFC) (2015CB856301) and the National Scientific Foundation of China (NSFC) (21571007, 21321001, 21101169, and 21778002) for financial support. This work was supported by the High-performance Computing Platform of Peking University.

Notes and references

1 (*a*) J. Beruter, J. P. Colombo and U. P. Schlunegger, *Eur. J. Biochem.*, 1975, **56**, 239–244; (*b*) H. Falk, *The Chemistry of Linear Oligopyrroles and Bile Pigments*, Springer, Vienna, 1989; (*c*) T. Yamaguchi, I. Shioji, A. Sugimoto, Y. Komoda and H. Nakajima, *J. Biochem.*, 1994, **116**, 298–303; (*d*) M. Bröring, C. D. Brandt and S. Stellwag, *Chem. Commun.*, 2003, **18**, 2344–2345.

2 (*a*) M. Bröring, S. Prikhodovski and C. D. Brandt, *J. Chem. Soc., Dalton Trans.*, 2002, **22**, 4213–4218; (*b*) M. Bröring, S. Prikhodovski, C. D. Brandt, E. C. Tejero and S. Köhler, *Dalton Trans.*, 2006, **2**, 200–208; (*c*) M. Bröring, S. Prikhodovski and E. C. Tejero, *Chem. Commun.*, 2007, **8**, 876–877; (*d*) S. Bahnmüller, J. Plotzitzka, D. Baabe, B. Cordes, D. Menzel, K. Schartz, P. Schweyen, R. Wicht and M. Bröring, *Eur. J. Inorg. Chem.*, 2016, **2016**, 4761–4768; (*e*) R. Gautam, J. J. Loughrey, A. V. Astashkin, J. Shearer and E. Tomat, *Angew. Chem., Int. Ed.*, 2016, **54**, 14894–14897; (*f*) E. Tomat, *Comments Inorg. Chem.*, 2016, **36**, 327–342; (*g*) R. Gautam, A. V. Astashkin, T. M. Chang, J. Shearer and E. Tomat, *Inorg. Chem.*, 2017, **56**, 6755–6762.

3 (*a*) J. L. Seganish and J. T. Davis, *Chem. Commun.*, 2005, 5781–5783, DOI: 10.1039/b511847f; (*b*) J. L. Sessler, L. R. Eller, W. S. Cho, S. Nicolaou, A. Aguilar, J. T. Lee, V. M. Lynch and D. J. Magda, *Angew. Chem., Int. Ed.*, 2005, **44**, 5989–5992; (*c*) P. A. Gale, *Acc. Chem. Res.*, 2011, **44**, 216–226.

4 (*a*) A. Srinivasan, T. Ishizuka and H. Furuta, *Angew. Chem., Int. Ed.*, 2004, **43**, 876–879; (*b*) S. Shimizu, R. Taniguchi and A. Osuka, *Angew. Chem., Int. Ed.*, 2005, **44**, 2225–2229; (*c*) Y. Kamimura, S. Shimizu and A. Osuka, *Chem. – Eur. J.*, 2007, **13**, 1620–1628; (*d*) S. Cinar, B. Temelli and C. Unaleroglu, *Tetrahedron Lett.*, 2014, **55**, 544–547;

(*e*) Y. Hisamune, K. Nishimura, K. Isakari, M. Ishida, S. Mori, S. Karasawa, T. Kato, S. Lee, D. Kim and H. Furuta, *Angew. Chem., Int. Ed.*, 2015, **54**, 7323–7327; (*f*) H. Mori, T. Tanaka, S. Lee, J. M. Lim, D. Kim and A. Osuka, *J. Am. Chem. Soc.*, 2015, **137**, 2097–2106; (*g*) Y. Rao, T. Kim, K. H. Park, F. Peng, L. Liu, Y. Liu, B. Wen, S. Liu, S. R. Kirk and L. Wu, *Angew. Chem., Int. Ed.*, 2016, **128**, 6454–6454; (*h*) J.-F. Wang, F. Ma, H.-L. Sun, J. Zhang and J.-L. Zhang, *J. Biol. Inorg. Chem.*, 2017, **22**, 727–737.

5 (*a*) Y. Ding, Y. Xie, X. Li, J. P. Hill, W. Zhang and W. Zhu, *Chem. Commun.*, 2011, **47**, 5431–5433; (*b*) Y. Ding, Y. Tang, W. Zhu and Y. Xie, *Chem. Soc. Rev.*, 2015, **44**, 1101–1112.

6 (*a*) G. M. Whitesides, E. E. Simanek, J. P. Mathias, C. T. Seto, D. N. Chin, M. Mammen and D. M. Gordon, *Acc. Chem. Res.*, 1995, **28**, 37–44; (*b*) V. G. Plotnikov, V. A. Sazhnikov and M. V. Alfimov, *High Energy Chem.*, 2007, **41**, 299–311; (*c*) C. Sutton, C. Risko and J.-L. Brédas, *Chem. Mater.*, 2015, **28**, 3–16; (*d*) K. Yuan, X. Wang, S. K. Mellerup, I. Kozin and S. Wang, *J. Org. Chem.*, 2017, **82**, 13481–13487.

7 (*a*) J. B. Birks, *Photophysics of Aromatic Molecules*, Wiley, London, 1970; (*b*) S. A. Jenekhe and J. A. Osaheni, *Science*, 1994, **265**, 765; (*c*) H. Nie, K. Hu, Y. Cai, Q. Peng, Z. Zhao, R. Hu, J. Chen, S.-J. Su, A. Qin and B. Z. Tang, *Mater. Chem. Front.*, 2017, **1**, 1125–1129.

8 (*a*) F. Würthner, *Chem. Commun.*, 2004, **35**, 1564–1579; (*b*) F. Würthner, T. E. Kaiser and C. R. Saha-Möller, *Angew. Chem., Int. Ed.*, 2011, **50**, 3376–3410; (*c*) K. Cai, J. Xie and D. Zhao, *J. Am. Chem. Soc.*, 2014, **136**, 28–31; (*d*) S. Herbst, B. Soberats, P. Leowanawat, M. Lehmann and F. Würthner, *Angew. Chem., Int. Ed.*, 2017, **129**, 2162–2165.

9 (*a*) D. C. Barber, R. A. Freitag-Beeston and D. G. Whitten, *J. Phys. Chem.*, 1991, **95**, 4074–4086; (*b*) D. Möbius, *Adv. Mater.*, 1995, **7**, 437–444; (*c*) H. von Berlepsch, C. Böttcher and L. Dähne, *J. Phys. Chem. B*, 2000, **104**, 8792–8799; (*d*) M. Shirakawa, S. Kawano, N. Fujita, K. Sada and S. Shinkai, *J. Org. Chem.*, 2003, **68**, 5037–5044; (*e*) A. E. Clark, C. Qin and A. D. Li, *J. Am. Chem. Soc.*, 2007, **129**, 7586–7595; (*f*) J. Gierschner and S. Y. Park, *J. Mater. Chem. C*, 2013, **1**, 5818–5832; (*g*) S. Choi, J. Bouffard and Y. Kim, *Chem. Sci.*, 2014, **5**, 751–755; (*h*) J. Mei, N. L. C. Leung, R. T. K. Kwok, J. W. Y. Lam and B. Z. Tang, *Chem. Rev.*, 2015, **115**, 11718–11940.

10 (*a*) Y. Kubota, T. Tsuzuki, K. Funabiki, M. Ebihara and M. Matsui, *Org. Lett.*, 2010, **12**, 4010–4013; (*b*) Y. Shigemitsu, T. Mutai, H. Houjou and K. Araki, *Phys. Chem. Chem. Phys.*, 2014, **16**, 14388–14395; (*c*) H. Wang, F. Chen, X. Jia, H. Liu, X. Ran, M. K. Ravva, F.-Q. Bai, S. Qu, M. Li, H.-X. Zhang and J.-L. Brédas, *J. Mater. Chem. C*, 2015, **3**, 11681–11688; (*d*) S. A. Sharber, R. N. Baral, F. Frausto, T. E. Haas, P. Muller and S. W. Thomas Iii, *J. Am. Chem. Soc.*, 2017, **139**, 5164–5174.

11 S. K. Dey, S. Datta and D. A. Lightner, *Monatsh. Chem.*, 2009, **140**, 1171–1181.

12 (*a*) Y. Hong, J. W. Lam and B. Z. Tang, *Chem. Soc. Rev.*, 2011, **40**, 5361–5388; (*b*) J. Mei, Y. Hong, J. W. Y. Lam, A. Qin, Y. Tang and B. Z. Tang, *Adv. Mater.*, 2015, **26**, 5429–5479.

13 (*a*) M. Stepień and L. Latos-Grazyński, *J. Am. Chem. Soc.*, 2002, **124**, 3838–3839; (*b*) T. D. Lash, A. M. Young, J. M. Rasmussen and G. M. Ferrence, *J. Org. Chem.*, 2011, **76**, 5636–5651; (*c*) B. Szyszko, L. Latos-Grazynski and L. Szterenberg, *Chem. Commun.*, 2012, **48**, 5004–5006; (*d*) T. D. Lash, *Org. Biomol. Chem.*, 2015, **46**, 7846–7878.

14 (*a*) C. Lee, W. Yang and R. G. Parr, *Phys. Rev. B: Condens. Matter Mater. Phys.*, 1988, **37**, 785–789; (*b*) A. D. Becke, *J. Chem. Phys.*, 1993, **98**, 5648–5652.

15 (*a*) P. C. Hariharan and J. A. Pople, *Theor. Chim. Acta*, 1973, **28**, 213–222; (*b*) M. M. Francl, W. J. Petro, W. J. Hehre, J. S. Binkley, M. S. Gordon, D. J. DeFree and J. A. Pople, *J. Chem. Phys.*, 1982, **77**, 3654–3665.

16 M. J. Frisch, G. W. Trucks, H. B. Schlegel, G. E. Scuseria, M. A. Robb, J. R. Cheeseman, G. Scalmani, V. Barone, G. A. Petersson, H. Nakatsuji, X. Li, M. Caricato, A. Marenich, J. Bloino, B. G. Janesko, R. Gomperts, B. Mennucci, H. P. Hratchian, J. V. Ortiz, A. F. Izmaylov, J. L. Sonnenberg, D. Williams-Young, F. L. F. Ding, J. G. F. Egidi, A. P. B. Peng, T. Henderson, D. Ranasinghe, V. G. Zakrzewski, N. R. J. Gao, G. Zheng, W. Liang, M. Hada, M. Ehara, K. Toyota, R. Fukuda, J. Hasegawa, M. Ishida, T. Nakajima, Y. Honda, O. Kitao, H. Nakai, T. Vreven, K. Throssell, J. J. A. Montgomery, J. E. Peralta, F. Ogliaro, M. Bearpark, J. J. Heyd, E. Brothers, K. N. Kudin, V. N. Staroverov, T. Keith, R. Kobayashi, J. Normand, K. Raghavachari, A. Rendell, J. C. Burant, S. S. Iyengar, M. C. J. Tomasi, J. M. Millam, M. Klene, C. Adamo, R. Cammi, J. W. Ochterski, R. L. Martin, K. Morokuma, O. Farkas, J. B. Foresman and D. J. Fox, *Gaussian 09, Revision D.01*, Gaussian, Inc., Wallingford CT, 2013.

17 J. Y. Shin, S. S. Hepperle, B. O. Patrick and D. Dolphin, *Chem. Commun.*, 2009, **10**, 2323–2325.

18 M. Kasha, H. R. Rawls and M. A. Elbayoumi, *Pure Appl. Chem.*, 1965, **11**, 371–392.

19 B. Heeg, P. A. DeBarber and G. Rumbles, *Appl. Opt.*, 2005, **44**, 3117–3124.

20 E. R. Johnson, S. Keinan, P. Mori-Sanchez, J. Contreras-Garcia, A. J. Cohen and W. T. Yang, *J. Am. Chem. Soc.*, 2010, **132**, 6498–6506.

21 (*a*) B. Jeziorski, R. Moszynski and K. Szalewicz, *Chem. Rev.*, 1994, **94**, 1887–1930; (*b*) E. G. Hohenstein and C. D. Sherrill, *J. Chem. Phys.*, 2010, **132**, 3430–1165; (*c*) E. G. Hohenstein, R. M. Parrish, S. C. David, J. M. Turney and H. F. Schaefer, *J. Chem. Phys.*, 2011, **135**, 174107; (*d*) T. M. Parker, L. A. Burns, R. M. Parrish, A. G. Ryno and C. D. Sherrill, *J. Chem. Phys.*, 2014, **140**, 094106.

22 A. M. Brouwer, *Pure Appl. Chem.*, 2011, **83**, 2213–2228.

23 T. Lu and F. Chen, *J. Comput. Chem.*, 2012, **33**, 580–592.

24 W. Humphrey, A. Dalke and K. Schulten, *J. Mol. Graphics*, 1996, **14**, 33–38.

25 (*a*) J. M. Turney, A. C. Simmonett, R. M. Parrish, E. G. Hohenstein, F. A. Evangelista, J. T. Fermann, B. J. Mintz, L. A. Burns, J. J. Wilke and M. L. Abrams, *Wiley Interdiscip. Rev.: Comput. Mol. Sci.*, 2012, **2**, 556–565; (*b*) R. M. Parrish, L. A. Burns, D. G. A. Smith, A. C. Simmonett, A. E. DePrince 3rd, E. G. Hohenstein, U. Bozkaya, A. Y. Sokolov, R. Di Remigio, R. M. Richard, J. F. Gonthier, A. M. James, H. R. McAlexander, A. Kumar, M. Saitow, X. Wang, B. P. Pritchard, P. Verma, H. F. Schaefer 3rd, K. Patkowski, R. A. King, E. F. Valeev, F. A. Evangelista, J. M. Turney, T. D. Crawford and C. D. Sherrill, *J. Chem. Theory Comput.*, 2017, **13**, 3185–3197.